Journal of Magnetic Resonance **152,** 149–155 (2001)
doi:10.1006/jmre.2001.2373, available online at http://www.idealibrary.com on IDEAL®

A Pulse EPR Study of Longitudinal Relaxation of the Stable Radical in γ-Irradiated L-Alanine

B. Rakvin,* N. Maltar-Strmečki,† P. Cevc,‡ and D. Arčon‡

*Ruđer Bošković Institute, P.O. Box 180, 10002, Zagreb, Croatia; †Faculty of Veterinary Medicine, P.O. Box 466, 10002, Zagreb, Croatia; and ‡Institute J. Stefan, P.O. Box 3000, 1001, Ljubljana, Slovenia

E-mail: rakvin@faust.irb.hr

Received February 6, 2001; revised May 8, 2001; published online July 6, 2001

The longitudinal relaxation rate of the first stable alanine radical, SAR1, was studied by employing pulse EPR technique over a wide temperature interval (5–290 K). The complex nonexponential recovery of the longitudinal magnetization in this temperature interval has been described with two characteristic relaxation times, $1/T_{1a}^*$ as the faster component and $1/T_{1b}^*$ as the slower component, respectively. It was shown that $1/T_{1a}^*$ is strongly affected by the CH_3 group dynamics of the SAR1 center. The complete temperature dependence of $1/T_{1a}^*$ was described by invoking several relaxation mechanisms that involve hindered motion of the CH_3 group from classical rotational motion to coherent rotational tunneling. It was shown that all relevant relaxation mechanisms are determined by a single correlation time with the potential barrier ($\Delta E/k = 1570$ K). On the other hand the temperature dependence of $1/T_{1b}^*$ is related to the motional dynamics of the neighborly NH_3 and CH_3 groups. We found a larger average potential barrier for this motion ($\Delta E/k = 2150$ K) corresponding to smaller tunneling frequencies of the neighbor groups.

Key Words: **pulse EPR; spin–lattice relaxation; L-alanine; paramagnetic center; proton tunneling.**

1. INTRODUCTION

The electron spin–lattice relaxation data in solids yield important information about the molecular groups dynamics. The relaxation data follow changes of the reorientation correlation times in the range of several orders of magnitude. Nevertheless such measurements have been so far rarely explored for the study of molecular dynamics. The reason lies in an extremely complex behavior of the individual magnetization relaxation curves, which are not simple one-exponential curves. A detailed systematic study of the electron spin–lattice relaxation data in a well-understood model system could provide a basis for studies of other more complex systems. In this respect we find γ-irradiated L-alanine as a good candidate. The longitudinal relaxation rates of the so-called first stable alanine radical ($HC\dot{C}H_3R$), SAR1, center (*1–3*) have been frequently studied by various pulse and nonlinear EPR techniques (*4–11*). These studies reveal that the motional averaging of the electron proton hyperfine splitting and a strong spectral diffusion mechanism are mostly responsible for the poorly understood relaxation rate behavior. A detailed microscopic picture of the origin of various relaxation mechanisms cannot be easily reconstructed due to significant disagreement in the experimental values of the measured parameters such as electron spin–lattice relaxation time, T_1, or rotational correlation time, $\tau = \tau_\infty \exp(\Delta E/kT)$ of the CH_3 group. For example, it can be demonstrated (*10*) that literature data for the CH_3 dynamics of the SAR1 center (*1, 4, 5, 7, 12*) differ in activation energy, $\Delta E/k$, from 1100 to 2100 K and even more for the preexponential factor, τ_∞, from 0.1 to 0.001 ps. On the other hand, several characteristic relaxation times were measured and origins of the corresponding relaxation mechanisms are not completely clear (*8, 9*). In order to elucidate some of these relaxation mechanisms it is essential to reverse the analysis: i.e., to determine as much as possible, an accurate value of τ and from it to calculate temperature dependence of various relaxation mechanisms.

Recently, EPR, transfer saturation EPR (TSEPR), and electron nuclear double-resonance (ENDOR) techniques have been employed (*11*) to obtain a more reliable τ value in the temperature region of fast motion of the CH_3 group (180–320 K). It was suggested (*11*) that the intermolecular motions can quite substantially influence the value of the measured correlation time τ and thus should not be neglected. This might explain the large discrepancies in the dynamical parameters reported previously for the CH_3 group of the SAR1 center.

The present study has been undertaken to examine the longitudinal relaxation rate of the SAR1 center over the temperature interval 5–290 K. The temperature dependence of the nonexponential relaxation rate is described by introducing several relaxation mechanisms that involve hindered motion of CH_3 groups from classical rotational motion to the coherent rotational tunneling. The electron spin–lattice relaxation measurements thus appear to be an unique tool for probing the molecular dynamics as one can follow the molecular group reorientational correlation times from the picosecond region around room temperature to the microsecond region at liquid helium temperatures. It is shown that all the relaxation mechanisms present can be

1090-7807/01 $35.00

described with two types of characteristic potential barriers in this entire temperature interval. The first one is related to the reorientation of the CH_3 group of the SAR1 center with an energy barrier 1570 K. The second energy barrier of about 2150 K represents the average reorientation potential barrier of the first neighbor groups (CH_3 and NH_3) to the SAR1.

2. EXPERIMENTAL

Single crystals of L-alanine were grown by slow evaporation from water solution at room temperature. Paramagnetic centers were produced by γ-ray irradiation (^{60}Co) with a dose of 10 kGy. The pulsed experiments were performed with a Bruker ELEXSYS 580 spectrometer. A simple inversion recovery technique (π–t_1–$\frac{\pi}{2}$–$\frac{\pi}{2}$–echo) has been used. A typical π pulse length was 128 ns. Each relaxation curve represents 1024 points when t_1 was regularly increased from 1000 ns to about 5 T_1. The field-swept spectra has been recorded with integration of the two-pulse echo signal ($\frac{\pi}{2}$–τ–$\frac{\pi}{2}$–τ–echo) while sweeping the external magnetic field over the resonant lines. Here τ was 200 ns and the integration gate was 100 ns.

3. RESULTS

When the magnetic field is applied along the L-alanine crystal *c* axis, the well-known quintet (1:4:6:4:1) spectrum is observed at room temperature due to the SAR1 center (*1*). The quintet structure originates from the three equivalent fast-rotating β-protons and one α-proton with an almost identical splitting. At low temperature ($T < 120$ K) the decrease in rotational motion of the CH_3 group leads to nonequivalent β-protons coupling and the spectrum splits further in the doublet structure. The change of the quintet as a function of temperature was described earlier (*1*) by employing modified Bloch equations and is related to the freezing out of the rotational motion of the CH_3 protons on the EPR time scale. The structure at low temperatures is unchanged below 120 K and it can be assumed that the CH_3 groups are frozen on the continuous wave EPR (CWEPR) time scale. Pulse EPR field-sweep spectra (Fig. 1) were obtained by recording the intensity of the electron spin echo signal as a function of the external magnetic field. They show a similar temperature behavior as was measured earlier by CWEPR. These spectra also show that the spin echo signals are largely due to the SAR1 center. (Particularly in the low-temperature region, $T < 30$ K, the field-sweep echo experiment significantly simplifies the observed broad structure of the CWEPR spectra by changing the separation time between echo-forming pulses).

The positions of the two outermost lines of the spectrum remain unchanged (proton spin states, $|---\rangle, |+++\rangle$) and they are invariant of CH_3 motions in the modified Bloch equation model (*1*). Thus, these lines can be good candidates for temperature-dependent studies of longitudinal relaxation rates for the SAR1 center at fixed magnetic field in the wide temperature interval. In the presence of spectral diffusion (*8*) it is

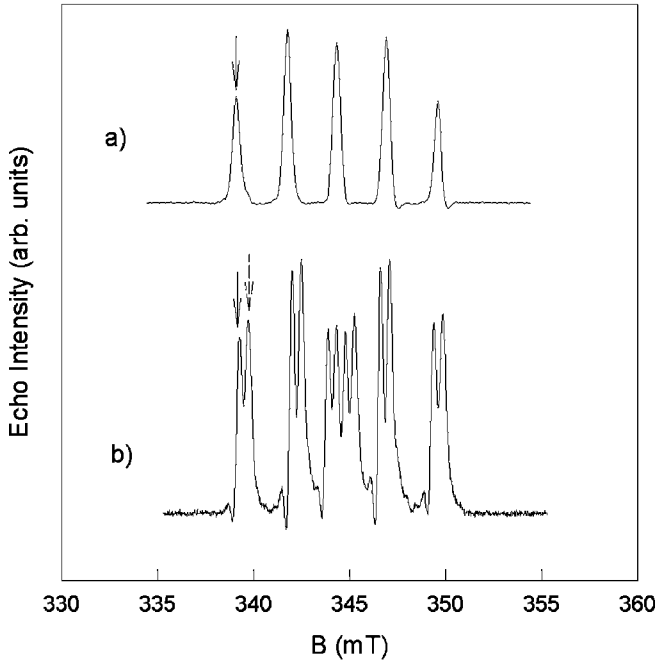

FIG. 1. Typical field-sweep echo EPR spectra for the first stable L-alanine radical for the magnetic field along $B \parallel c$ (a) at 287 K and (b) at 25 K. The arrows denote magnetic field positions for the $|---\rangle$ (solid) and $|+--\rangle$ (dashed) proton hyperfine components.

convenient to employ a standard inversion recovery pulse sequence (*13*) for measurements of longitudinal relaxation rates. In the pulse sequence, the evolution time and other parameters were carefully checked to obtain more reliable relaxation rates especially in the low-temperature region. The typical electron magnetization recovery curve (taken at the low-field hyperfine component denoted by the arrow in Fig. 1) is shown in Fig. 2 and exhibits a multiexponential shape

$$R(t) = \sum_j A_j^* \lfloor 1 - S_j \exp(-t/T_{1j}^*) \rfloor, \qquad [1]$$

where T_{1j}^* represents the characteristic longitudinal relaxation time. Most of these curves can be described with biexponential function. We have therefore attempted to fit all magnetization curves with a biexponential formula. As a result, two different characteristic relaxation times were observed, and we name them $1/T_{1a}^*$ and $1/T_{1b}^*$. One expects that the detected recovery curves will show the presence of different relaxation processes due to the strong spectral diffusion via neighboring protons that is present in the system. This is because the entire EPR spectrum is too wide to be completely saturated. In this case, as was discussed earlier (*8*) it is expected that the faster relaxation rate is always more effective than the slower relaxation rate.

The experimental results for both relaxation components in the temperature interval 5–290 K are shown in Fig. 3. For the relaxation rate measured at room temperature it can be noted

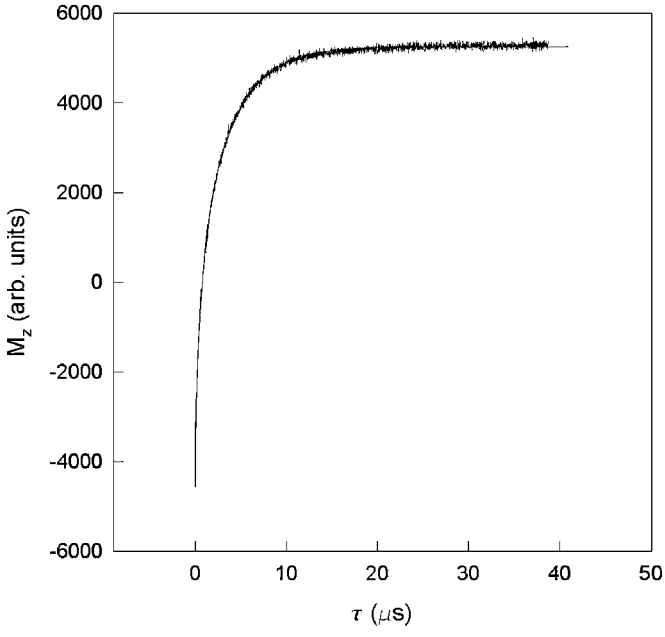

FIG. 2. Saturation recovery spectrum of SAR1 measured for the $|---\rangle$ hyperfine proton component at 40 K. The continuous line represents a biexponential fit to the Eq. [1].

that deduced values ($T_{1a}^* = 2.1\ \mu$s, $T_{1b}^* = 21.2\ \mu$s) show the same order of magnitude as the values measured earlier (*6*, *8*, *9*). However, over a wide temperature region, both components exhibit complex temperature dependence with some similarities. It

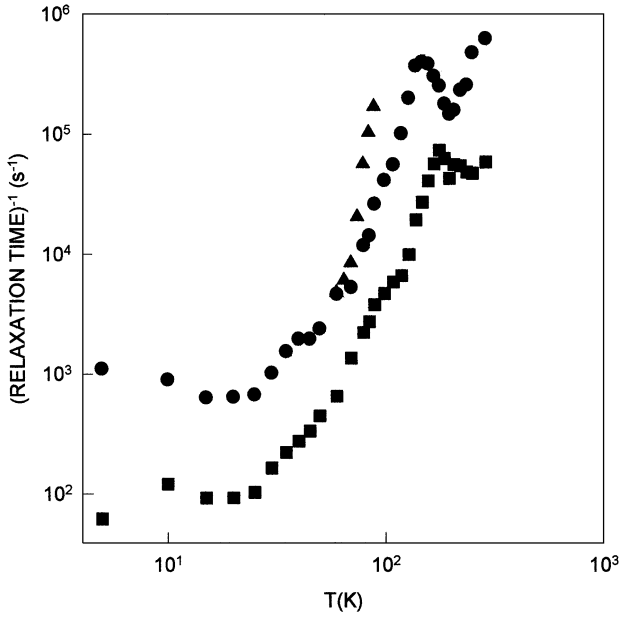

FIG. 3. Characteristic longitudinal relaxation times (obtained for the low field hyperfine component denoted by the continuous arrow in Fig. 1), $1/T_{1a}^*$ (circles) and $1/T_{1b}^*$ (squares) evaluated from recovery spectra at various temperatures. Triangles represent $1/T_{1a}^*$ obtained from the $|+--\rangle$ hyperfine component.

is thus convenient to use the notation for the two relaxation times as T_{1a}^* for the shorter relaxation and T_{1b}^* for the longer relaxation time in the whole temperature interval. Two maxima at higher temperatures (∼160 K) and an unexpected rapid relaxation behavior at lower temperatures of the fast- and the slow-relaxation components (Fig. 3) indicate that several different relaxation mechanisms are active in the entire temperature range.

In the low-temperature range the relaxation rate was also measured on the second nearest EPR line to the low field line ($|+--\rangle$, the magnetic field position denoted by dashed arrow in Fig. 1b. This step was important in order to check the sensitivity of the measured relaxation rate due to the hindered motion of the CH_3 group. Normally the second line of the spectrum is affected by the proton exchange and one expects that its longitudinal relaxation rate is directly enhanced by the rotation correlation motion of the CH_3 group (*4*). It should be noted that the relaxation curves for the second line could be measured only up to 90 K, where the intensity of the second line collapsed due to fast proton exchange. Indeed, for this EPR line the measured longitudinal relaxation rate is enhanced as is shown in Fig. 3 (triangles). One notes that difference in the longitudinal relaxation between the two lines can be detected at temperature significantly lower (down to ∼60 K) than that of the changes in the EPR spectrum caused by freezing out of the molecular group reorientations, which started at around 120 K. Thus, reliable information on τ for the CH_3 group in the region of very slow motion is expected and can help to deduce the real nature of the unknown relaxation mechanism. However, below ∼60 K the two relaxation rates become identical within the experimental error bar. We thus conclude that below ∼60 K this additional relaxation channel becomes ineffective and the two lines have the same T_1^*.

4. DISCUSSION

4.1. The Spin Hamiltonian

The temperature dependence of the longitudinal relaxation rate, as described above, exhibits very complex behavior, and it is approximated with two different characteristic relaxation times T_{1a}^* and T_{1b}^*. One expects that the functional temperature dependence of each of these relaxation times is dominated by dynamical motion of the methyl groups. The spin Hamiltonian for methyl group protons with respect to the unpaired electron contains the terms (*14*, *15*)

$$H = \upsilon_e S_z + \upsilon_n \sum_k I_{kz} + \sum_k \mathrm{S}\mathbf{T}_k \mathrm{I}_k + H_n - 2J_\upsilon \sum_{j<k} \mathrm{I}_k \mathrm{I}_j, \quad [2]$$

where υ_e and υ_n are the electron and nuclear Larmor frequencies. $\mathbf{T_k}$ is the electron–nuclear hyperfine interaction, END, for the kth nucleus, and H_n is the nucleus–nucleus dipolar interaction, NND. The last term describes the proton exchange contribution for the υth libration level of the methyl group. The first

three terms are usually employed to describe CH_3 relaxation in the fast-motion regime involving classical jumping of protons between the three potential wells. The quantum aspect of CH_3 dynamics inside of a potential barrier involves the last term (Eq. [2]). The tunneling splitting for the ground libration level ($3J_0$) and other excited levels can be calculated from the height of the potential barrier by using the stationary Schrödinger equation for the hindered rotor (*16, 17*). In what follows we will describe the contributions of the individual terms in Eq. [2] to the spin–lattice relaxation of the SAR1 center.

4.2. Temperature Dependence of the $1/T_{1a}^*$ Relaxation Rate

An indication that the dominant relaxation mechanism in the fast-motion regime of the CH_3 groups arises due to electron–proton cross-relaxation terms following from the nonsecular term ($\Delta m_s = \pm 1, \Delta m_I = \mp 1$) in the Hamiltonian (Eq. [2]) was suggested in the previous EPR (*1*) and ENDOR (*5, 11*) studies. The corresponding relaxation rate is in this case (*5*)

$$1/T_{1x} \approx j(\omega_e) = \frac{b^2}{16\omega_e} \frac{2\tau\omega_e}{1+\tau^2\omega_e^2}, \qquad [3]$$

where $(b/2\pi) = 140$ MHz represents a constant connected with electron–proton isotropic coupling T_k and $\omega_e = 2\pi\upsilon_e$ represents electron Larmor frequency. Since the splitting constant b is the largest interaction constant in Hamiltonian [2], the contribution of this term is expected to be dominant in the fast-motion regime of CH_3 group. Thus, the position of the corresponding maxima on the temperature scale can be easily correlated with one of the maxima from the experimental data if the reliable value for τ is known. In the low-temperature range we use the advantage of the independent measurement of T_{1a}^* for $|---\rangle$ and for $|+--\rangle$ EPR lines. The results were used to directly obtained τ in the low-temperature region:

$$(1/T_{1a}^*)_{|+--\rangle} = (1/T_{1a}^*)_{|---\rangle} + 1/\tau. \qquad [4]$$

The dotted line in Fig. 4 is the fit of the relaxation rate $1/T_{1a}^*$ for $|+--\rangle$ EPR line (triangles) by using Eq. [4] and the correlation time τ ($\tau_\infty = 0.12 \pm 0.06$ ps, $\Delta E/k = 1570 \pm 45$ K). The agreement between experiment and fit is within the experimental error and the values of τ agree with those of recently measured and revised τ values in the fast-motion regime (*11*). The obtained value of τ was used to calculate position and maxima of the cross-relaxation term (Eq. [3]). A fitted constant of $(b/2\pi) = 136$ MHz satisfied the dependence of $1/T_{1a}^*$ relaxation rate at high temperatures (i.e., in the temperature interval between 200 and 250 K) as shown by the dashed curve w_e in Fig. 4. Good agreement between the experimental points and the theoretical prediction proves that the electron–nuclear spin flip mechanism of the nearest CH_3 group is the leading mechanism in the relaxation of $1/T_{1a}^*$ in the high-temperature interval.

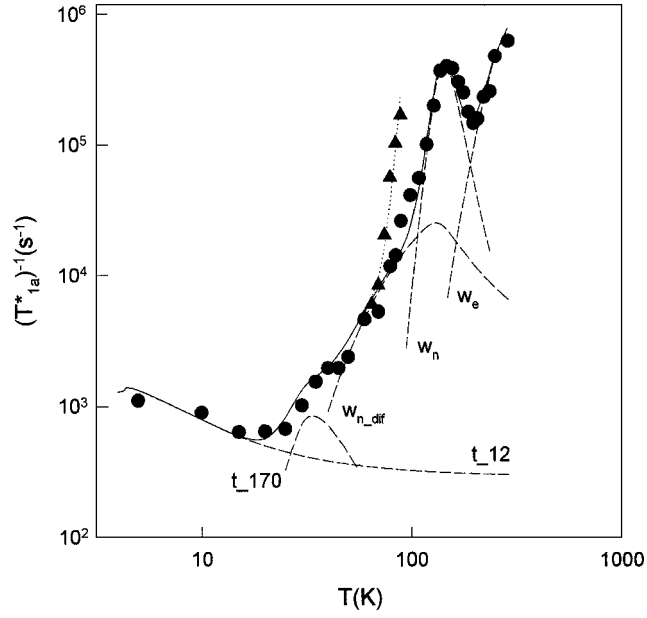

FIG. 4. Temperature dependence of the experimentally obtained $1/T_{1a}^*$ (circles) and that calculated (continuous curve). The most prominent contributions for the particular relaxation mechanisms are described with the dashed curves and denoted as w_e, electron–proton spin flip; w_n, END pseudo-secular, w_{n_dif}, proton diffusion; t_12, and t_170, the first and the second tunneling contributions. $1/T_{1a}^*$ (triangles) obtained from the $|+--\rangle$ hyperfine component are fitted to Eq. [4] and it is shown as the dotted line.

For further analysis of these data it is important to note that contributions from the all other nonsecular terms are negligible due to small anisotropic coupling in comparison to the isotropic coupling of the CH_3 group (*1*).

The second important term that contributes to the longitudinal relaxation rate is the pseudo-secular part ($\Delta m_s = 0$, $\Delta m_I = \pm 1$) with the proton transition in the vicinity of the nuclear Larmor frequency υ_n. The contribution of this term is derived from the END coupling, and can be written in the form

$$(1/T_{1n})_{PS}^{END} = \frac{C_{PS}^{END}}{2\omega_n} \frac{2\omega_n\tau}{1+\omega_n^2\tau^2} = (1/T_{1n})_{MAX} \frac{2\omega_n\tau}{1+\omega_n^2\tau^2}. \qquad [5]$$

For the CH_3 group, the isotropic hyperfine splitting is large, $a \approx 70$ MHz and the nuclear Larmor frequency should be replaced with the nuclear transition frequencies $\upsilon_{n\pm} = \upsilon_n \pm \frac{a}{2}$. In the END relaxation rate the anisotropic coupling is on the order of a few megahertz for each proton and it is small compared to the isotropic coupling. However, the cumulative contribution of the END relaxation can be significant at lower temperatures ($T < 200$ K) in comparison to cross-relaxation terms and all other terms that include ω_e, because the maximum is proportional to $1/\omega$ and ($1/\omega_n \gg 1/\omega_e$). A maximum of the relaxation rates around 160 K corresponds to the $(1/T_{1n})_{PS}^{END}$ mechanism as can be seen in Fig. 4 (dashed curve denoted by w_n). Using

TABLE 1
Parameters from Eqs. [5], [6], and [8] Fitted to the Measured $1/T_{1a}^*$ and $1/T_{1b}^*$ Values of the SAR1 Paramagnetic Center

	$C^{\mathrm{END}}(\mathrm{s}^{-2})$	$R_{\mathrm{MAX}}^{\mathrm{SD}}(\mathrm{s}^{-1})$	$\tau_{\infty 1}^{l}$(ps)	E_1^l/k (K)	$3\Delta_1/\hbar$ (s^{-1})	$\tau_{\infty 2}^{l}$(ps)	E_2^l/k (K)	$3\Delta_2/\hbar$ (s^{-1})
$1/T_{1a}^*$	8.87×10^{13}	2.5×10^{4}	90	170	4.8×10^{6}	990	12	6.0×10^{6}
$1/T_{1b}^*$	9.85×10^{12}	1.3×10^{4}	81	190	3.0×10^{6}	870	26	3.0×10^{6}

the same τ for the cross-relaxation terms, the fitting constant $C_{\mathrm{Ps}}^{\mathrm{END}}$ is determined for the $1/T_{1a}^*$ relaxation rate (Table 1). We stress once again that the position of the maximum relaxation rates is obtained from ENDOR transition frequencies and satisfied previously determined τ. The only free-fitting parameter is $C_{\mathrm{PS}}^{\mathrm{END}}$. Thus, the detected $(1/T_{1\mathrm{n}})_{\mathrm{PS}}^{\mathrm{END}}$ with the corresponding coupling constant ~1.5 MHz can be identified with the relaxation mechanism due to the averaging out of the anisotropy splitting of the CH_3 group and is responsible for the electron spin–lattice relaxation in the intermediate region between 120 and 200 K.

Upon further cooling, the change in the $1/T_{1a}^*$ temperature behavior can be clearly noted below 100 K, and one expects that some other relaxation mechanism takes over in this region. Following earlier investigation of the relaxation rates of the spin probes in the slow-motion region (*18*), we propose that this mechanism is due to the proton spin diffusion. Its contribution to the electron spin–lattice relaxation has been calculated previously (*18*) and can be approximated with the form

$$(1/T_{1\mathrm{n}})^{\mathrm{SD}} = (R)_{\mathrm{MAX}}^{\mathrm{SD}}\left(\frac{2\omega_{\mathrm{n}}\tau}{1+(\omega_{\mathrm{n}}\tau)^{3/2}}\right)^{1/4}. \qquad [6]$$

The origin of this term is associated with proton spin-flip rate of the CH_3 group in the Hamiltonian (Eq. [2]). Still using the same τ and nuclear Larmor frequency, the $(1/T_{1\mathrm{n}})^{\mathrm{SD}}$ value well describes the temperature dependence of $1/T_{1a}^*$ in the low-temperature interval (30–60 K) as shown by dashed curve (denoted as $w_{\mathrm{n\_dif}}$) in Fig. 4. The obtained $(R)_{\mathrm{MAX}}^{\mathrm{SD}} = 2.5\times10^{4}\ \mathrm{s}^{-1}$ is in the expected range for proton diffusion (*18*).

It thus turns out that the relaxation mechanisms based on the CH_3 group rotational motions determine the temperature dependence of $1/T_{1a}^*$ over the large temperature range. However at the lowest temperatures, the above conjecture fails to describe the $1/T_{1a}^*$ temperature dependence. As shown above, the dominant contribution to relaxation process is related to the proton hopping and diffusion type of dynamics. At low temperatures the proton motion is restricted to the proton tunneling inside the hindered potential. We now try to estimate the contribution of this type of proton motion to the electronic spin–lattice relaxation. The tunneling model of the CH_3 protons was suggested by Clough (*19*) to describe the contribution of tunneling to NMR T_1 proton relaxation. We use their model here to describe a proton relaxation rate in the low-temperature region:

$$\begin{aligned}(1/T_{1\mathrm{n}})^{\mathrm{TU}} &= C_{\mathrm{pp}}(\pi L(\omega_{\mathrm{n}}) + 4\pi L(2\omega_{\mathrm{n}}))\\ L(\omega) &= \frac{1}{2}(G(\omega)+G(-\omega))\\ G(\omega) &= \frac{(12p_1+9p_1\hbar^{-1}\Delta)M-(9\hbar^{-2}\Delta^2-3\omega^2+9p_1^2)N}{3\pi(M^2+N^2)}\\ M &= \omega\left(9\hbar^{-2}\Delta^2-\omega^2+3p_1^2\right)\\ N &= 4p_1\omega^2-9p_1\hbar^{-2}\Delta^2+3\hbar^{-1}\Delta p_1\omega. \end{aligned} \qquad [7]$$

The constant C_{pp} represents the proton–proton interaction and $3\Delta/h = 3J$ is the tunneling frequency connected with notation in Eq. [2]. The correlation time, $1/p_1 = \tau^l = \tau_\infty^l \exp(E^l/kT)$, obeys the Arrhenius relation between the ground state and the first excited vibrational states of the CH_3 group. In the NMR case the spectral density for the NND relaxation rate exhibits the same functional form as the spectral density for the END pseudo-secular term relaxation rate given in Eq. [5]. The difference between these rates is only in the value of the interaction constant. In order to describe tunneling effects one can expand the spectral density simply by adding $L(\omega)$ terms from Eq. [7]. The same expanded spectral density can be introduced in Eq. [5] to obtain the electron–proton relaxation rate additionally affected by tunneling:

$$(1/T_{1\mathrm{n}})^{\mathrm{END}} = C_{\mathrm{PS}}^{\mathrm{END}}\left(\frac{\tau}{1+\omega_{\mathrm{n}}^2\tau^2}+\pi L(\omega_{\mathrm{n}})+4\pi L(2\omega_{\mathrm{n}})\right). \qquad [8]$$

In the fitting strategy we used $C_{\mathrm{PS}}^{\mathrm{END}}$ obtained by fitting the high-temperature data. The parameters $3\Delta/\hbar$, τ_0^l, and E^l were now treated as variable parameters in Eq. [8] and the fit in the low-temperature region leads us to the E^l, τ_∞^l, and Δ values listed in Table 1. The two fits with maxima around 6 and 35 K (dashed curves t_12 and t_170) are estimated and shown in Fig. 4. The tunneling splitting with corresponding excitation states was obtained. The obtained values of tunneling frequencies are similar in magnitude ($3\Delta/\hbar \approx 1$ MHz), and expected for the values of a hindered potential with barrier height of ≈1500 K (*16*, *17*). Here it should be noted that besides the approximations that were employed in Eq. [8] the value of the tunneling frequencies deduced can appear as an average of tunneling frequencies if

the population of higher libration states are involved (*20*). Thus, with all the above-mentioned relaxation mechanisms, the $1/T_{1a}^{*}$ value is described over a wide temperature interval as shown by the continuous curve in Fig. 4. It is important to note that the fast component of the relaxation rate dominates and arises from the motional dynamics of the nearest CH_3 over a wide frequency range from proton hopping over the hindered potential to the proton tunneling inside this potential.

We shall mention here that the magnetization recovery curve at low-temperature range starts to deviate from the biexponential curve and can be satisfactory fitted only by involving more exponents. The most likely reason for this is that at low temperatures the nuclear spin–lattice relaxation couples more than two lines together. In this case multiexponential decay is expected. Nevertheless we expect that the values extracted and presented here represent the average values of the slow- and fast-relaxation components and as such their general temperature dependence should be correct, although precise value of the fitting parameters might be unreliable.

4.3. Temperature Dependence of the $1/T_{1b}^{*}$ Relaxation Rate

Now, in accord with the above discussion, the slow-relaxation components $1/T_{1b}^{*}$ can be simply assigned to the relaxation processes due to rotational motional dynamics of neighboring CH_3 and NH_3 groups in the lattice. Of course, in that case the slow component of the relaxation rate is dominated by proton dynamics as was the case for the fast component. Thus, one expects that the same type of mechanisms of relaxation should be involved in the wide temperature interval. Indeed, temperature dependence of $1/T_{1b}^{*}$ is described by using the same type of relaxation mechanisms as in the case of the fast component. The fitting curves with best-fitted τ ($\tau_\infty = 0.09 \pm 0.06$ ps, $\Delta E/k = 2150 \pm 50$ K) using the cumulative relaxation rate description of $1/T_{1b}^{*}$ are shown in Fig. 5. The additional fitting parameters of Eqs. [5], [6], and [8] are given in Table 1. According to expectations for distant protons all interaction constants are weaker due to smaller electron spin density than to closer CH_3 protons. However, one notes significantly different τ ($\Delta E/k = 2150$ K) for these distant proton groups. A τ with similar potential barrier was obtained in the recent investigation of SAR1 dynamics (*11*) by employing transfer saturation EPR and it was attributed to the dynamics of the neighboring CH_3 and NH_3 groups. It is also interesting to note that NMR study yields $\Delta E/k \approx 2700$ K for τ of CH_3 and NH_3 groups in nonirradiated L-alanine (*21*). All the distant protons exhibit hopping and tunneling in the hindered potential with a barrier higher than that of the nearest CH_3 group. This higher barrier requires a smaller tunneling splitting, which was indeed obtained in the fitting procedure of the well-resolved maximum at 10 K.

Tunneling of CH_3 groups was studied earlier (*16, 17, 19*) for paramagnetic centers possessing a low hindered potential ($\Delta E/k \approx 200$ K) for CH_3 when the rotation rate is sufficiently rapid even at low temperature to the average anisotropic coupling. In this case a significantly larger tunneling frequency is

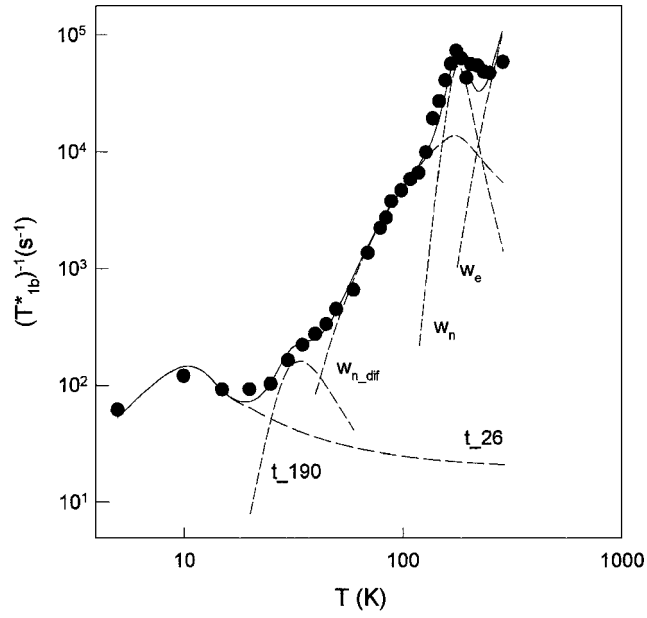

FIG. 5. Temperature dependence of experimentally obtained $1/T_{1b}^{*}$ (circles) and that calculated (continuous curve). The most prominent contributions for the particular relaxation mechanisms are described with the dashed curves and denoted as w_e, electron–proton spin flip; w_n, END pseudo-secular, w_{n_dif}, proton diffusion; t_26, and t_190, the first and the second tunneling contributions. The contribution of w_e is only noted as this term and the corresponding constant are not included in Table 1.

expected ($3J \gg a$). The effect of such a large tunneling frequency can be seen on the EPR spectrum as a splitting of the second and the third lines of the (1:3:3:1) fast-motion CH_3 spectrum (*16, 22*). In such a case, an EPR spectrum is not convenient for estimation of the tunneling splitting. However it can be estimated by measuring second-order contributions in an ENDOR spectrum (*14, 15*). In the case when ($3J \leq a$), the tunneling splitting frequency cannot be resolved inside the degenerated lines. The relaxation rate, on the other hand, is sensitive to even a small tunneling frequency through the proton relaxation terms and can thus provide complementary information about the low-temperature proton dynamics.

Two distinct longitudinal relaxation times of the SAR1 center were detected in earlier studies (*8, 9*), although the underlying mechanism was not proposed. The possibility that the electron–proton cross-relaxation mechanism due to the hindered motion of CH_3 is responsible for the faster longitudinal relaxation component was suggested recently (*11*). This suggestion was based on the measurements of T_1 components as a function of microwave frequencies at room temperature (*9*). The present data obtained by pulse EPR supports this suggestion (*11*) and moreover clearly reveals several other relaxation mechanisms, which are involved over a wide temperature interval.

5. CONCLUSION

We have performed a detailed analysis of the electron relaxation rates of the SAR1 paramagnetic center in γ-irradiated

L-alanine. By employing the inversion recovery pulse EPR technique the longitudinal relaxation rate obtained exhibits complex behavior over a wide temperature interval. Several relaxation mechanisms such as proton tunneling, proton diffusion, and hindered hopping of protons for corresponding hindered potential were involved in describing this complex relaxation process. In comparison with earlier studies, where detection and discussion were restricted to large ($3J \gg a$) tunneling splitting, the evidence for a small tunneling splitting ($3J \leq a$) is presented and discussed in this work. The relaxation mechanisms involved show that the largest effect of tunneling is detected by the pseudo-secular part of the END Hamiltonian. It should be noted here that in an earlier model of a spin–lattice relaxation mechanism involving tunneling modes for the trapped radical in glassy matrix, the pseudo-secular part of END was neglected (*23*). However, the characteristic properties of the temperature behavior of $(T_1)^{-1}$ of methyl radicals in glassy organic matrices exhibit similar values and similar behavior as the longitudinal relaxation of the SAR1 center at low temperatures (5–100 K) (*24*), and it might be reinterpreted in accordance with the SAR1 model.

REFERENCES

1. I. Miyagawa and K. Itoh, Electron spin resonance of irradiated single crystals of alanines: Hindered rotation of the methyl group in a free radical, *J. Chem. Phys.* **36,** 2157 (1962).
2. S. Kuroda and I. Miyagawa, ENDOR study of an irradiated crystal of L-Alanine: Enviroment of the stable $CH_3CHCO_2^-$ radical, *J. Chem. Phys.* **76,** 3933 (1982).
3. E. Saugstuen, E. O. Hole, S. R. Haugedal, and W. H. Nelson, Alanine radicals: Structure determination by EPR and ENDOR of single crystals X-irradiated at 295 K, *J. Phys. Chem. A,* **101,** 9763 (1997).
4. S. A. Dzuba, K. M. Salikhov, and Yu. D. Tsvetkov, Slow rotations ($\tau \geq 10^{-5}$ s) of methyl groups in radicals studied by pulse ESR spectroscopy, *Chem. Phys. Lett.* **79,** 568 (1981).
5. M. Brustolon, T. Cassol, L. Micheletti, and U. Segre, Methyl dynamics studied by ENDOR spectroscopy: a new method, *Molec. Phys.* **57,** 1005 (1986).
6. K. Nakagawa, S. S. Eaton, and G. R. Eaton, Electron spin relaxation times of irradiated alanine, *Appl. Radiat. Isot.* **44,** 73 (1993).
7. R. Angelone, C. Forte, and C. Pinzino, Relaxation Time Measurements by Longitudinally Modulated ENDOR Spectroscopy on Irradiated l-alanine Single Crystal, *J. Magn. Reson. A* **101,** 16 (1993).
8. M. Brustolon and U. Segre, Electron spin-lattice relaxation time and spectral diffusion in γ-irradiated L-Alanine, *Appl. Magn. Reson.* **7,** 405 (1994).
9. B. T. Ghim, J-K. Du, S. Pfenninger, G. A. Rinard, R. W. Quine, S. S. Eaton, and G. R. Eaton, Multifrequency electron paramagnetic resonance of L-Alanine, *Appl. Radiat. Isot.* **47,** 1235 (1996).
10. B. Rakvin, Double modulation ESR study of irradiated alanine, *Appl. Radiat. Isot.* **47,** 1251 (1996).
11. B. Rakvin and N. Maltar-Strmečki, Study of relaxation rates of stable paramagnetic centers in γ-irradiated alanine, *Spectrochim. Acta A* **56,** 399 (2000).
12. A. Horsfield, J. R. Morton, and D. H. Whiffen, The electron paramagnetic resonance spectrum of CH3CH(CO2H) beetwen 100 K and 200 K, *Mol. Phys.* **5,** 115 (1962).
13. A. Schweiger, Pulsed electron spin resonance spectroscopy: Basic principles, techniques, and examples of applications, *Angew. Chem. Int. Ed. Engl.* **30,** 265 (1991).
14. S. Clough and F. Poldy, Study of tunneling rotation of methyl groups by electron spin resonance and electron nuclear double resonance, *J. Chem. Phys.* **51,** 2076 (1969).
15. F. Bonon, M. Brustolon, A. L. Maniero, and U. Segre, An ENDOR study of the temperature dependence of methyl tunneling, *Chem. Phys.* **161,** 257 (1992).
16. J. H. Freed, Quantum effects of methyl-group rotations in magnetic resonance: ESR splittings and linewidths, *J. Chem. Phys.* **43,** 1710 (1965).
17. A. R. Sørnes and N. P. Benetis, The EPR spectrum of the general $\rangle \dot{C} - CX_3$ quantum rotor, *Chem. Phys.* **226,** 151 (1998).
18. B. H. Robinson, D. A. Haas, and C. Mailer, Molecular dynamics in liquids: Spin–lattice relaxation of nitroxide spin labels, *Science* **263,** 490 (1994).
19. S. Clough, Proton spin–lattice relaxation due to tunneling motions, *Solid State Phys.* **4,** 2180 (1971).
20. W. Müller-Warmuth, R. Schüler, M. Prager, and A. Kollmar, Rotational tunneling in methylpyridines as studied by NMR relaxation and inelastic neutron scattering, *J. Chem. Phys.* **69,** 2382 (1978).
21. E. R. Andrew, W. S. Hinshaw, M. G. Hutchins, and R. O. I. Sjöblom, Proton magnetic relaxation and molecular motion in polycrystalline amino acids, II. Alanine, isoleucine, methionine, norleucine, threonine and valine, *Mol. Phys.* **32,** 795 (1976).
22. R. B. Davidson and I. Miyagawa, ESR study of quantum tunneling of a methyl group: A simple tunneling model, *J. Chem. Phys.* **52,** 1727 (1970).
23. M. K. Bowman and L. Kevan, An electron spin–lattice relaxation mechanism involving tunneling modes for trapped radicals in glassy matrices. Theoretical development and application to trapped electrons in γ-irradiated ethanol glasses, *J. Phys. Chem.* **81,** 456 (1977).
24. J. Michalik and L. Kevan, Temperature dependence of electron spin-lattice relaxation of methyl radicals in glassy organic matrices: Relation to environmental dynamics and radical decay, *J. Phys. Chem.* **68,** 5325 (1978).